

RSC Advances



This is an *Accepted Manuscript*, which has been through the Royal Society of Chemistry peer review process and has been accepted for publication.

Accepted Manuscripts are published online shortly after acceptance, before technical editing, formatting and proof reading. Using this free service, authors can make their results available to the community, in citable form, before we publish the edited article. This *Accepted Manuscript* will be replaced by the edited, formatted and paginated article as soon as this is available.

You can find more information about *Accepted Manuscripts* in the [Information for Authors](#).

Please note that technical editing may introduce minor changes to the text and/or graphics, which may alter content. The journal's standard [Terms & Conditions](#) and the [Ethical guidelines](#) still apply. In no event shall the Royal Society of Chemistry be held responsible for any errors or omissions in this *Accepted Manuscript* or any consequences arising from the use of any information it contains.

1 **A novel graphene oxide coated biochar composite: synthesis,**
2 **characterization and application for Cr(VI) removal**

3 Mei-rong Shang^{a,b}, Yun-guo Liu^{a,b,*}, Shao-bo Liu^c, Guang-ming Zeng^{a,b}, Xiao-fei
4 Tan^{a,b}, Lu-hua Jiang^{a,b}, Xi-xian Huang^{a,b}, Yang Ding^{a,b}, Yi-ming Guo^d, Shu-fan
5 Wang^{a,b}

6 ^a College of Environmental Science and Engineering, Hunan University, Changsha
7 410082, P.R. China

8 ^b Key Laboratory of Environmental Biology and Pollution Control (Hunan
9 University), Ministry of Education, Changsha 410082, P.R. China

10 ^c College of Metallurgy and Environmental Research, Central South University,
11 Changsha 410004, P.R. China

12 ^d Yi-Ming Guo School of Economics and Management, Shanghai Maritime University,
13 1550 Haigang Ave, Shanghai 201306 P.R.China.

14 * Corresponding author: Yun-guo Liu; Tel.: +86 731 88649208; Fax: +86 731
15 88822829; E-mail address: liuyunguo824@sina.com.

Abstract

In the current work, graphene oxide coated water hyacinth biochar composite (WHB-GO) was synthesized to remove Cr(VI) from aqueous solution. The biomass feedstock was firstly treated with graphene oxide and then annealed at 300 °C in a quartz tube furnace under N₂ atmosphere. After synthesis, the full characterization with various techniques (SEM, FT-IR, XPS and BET) were used to analyze the properties of the adsorbent and the sorption mechanisms of Cr(VI). The effects of pH, ionic strength, sorption kinetics, isotherms and thermodynamics, as well as comparison and regeneration experiments were also investigated. The results indicated that the adsorption capacity was significantly influenced by pH and ionic strength. The maximum adsorption capacity (150.02 mg g⁻¹) of the WHB-GO was obtained at pH 2.0 and 50 °C. Besides, the sorption data could be fitted well by pseudo-second-order and Freundlich models. The thermodynamic studies indicated that the adsorption reaction was a spontaneous and endothermic process. The enhanced adsorption of Cr(VI) on the WHB-GO was mainly controlled by electrostatic attraction and reduction of Cr(VI) coupled with Cr(III) complexation. The regeneration study revealed that WHB-GO could be reused almost six times without loss of their activity in adsorption tests. Overall, WHB-GO can be used as a novel, facile, and low-cost sorbent for the removal of Cr(VI) from aqueous solution.

Keywords:

Novel composite; Graphene oxide; Adsorption; Hexavalent chromium; Reduction

37 1. Introduction

38 In recent years, the heavy metal ions at high concentrations in water systems
39 have posed a potential threat to human beings and living organisms due to their
40 bioaccumulation and decomposition difficulty in food chains¹. Chromium is one of
41 the most widespread heavy metals in the environment. As a major pollutant,
42 chromium mainly exists in two stable forms in water: Cr (III) and Cr(VI).² However,
43 Cr(VI) is especially poisonous, which was 100 times greater than Cr(III) in toxicity.
44 Thus, hexavalent chromium can cause many serious health problems for human
45 beings (e.g., skin irritations, lung cancer, and viscera damage).³ So, developing an
46 effective method to remove Cr(VI) from effluent is of great importance to the public
47 health and ecological system. Until now, the methods of removing Cr(VI) are
48 miscellaneous, such as electrocoagulation,⁴ reverse osmosis (RO),⁵ ion exchange,⁶
49 redox reaction,⁷ membrane separation,⁸ and adsorption.⁹ Among these methods,
50 adsorption is one of the most popular and effective option, due to its
51 cost-effectiveness, simple operation and least waste generation.¹⁰

52 Biochar is an easily acquiring adsorbent, which has been increasingly used to
53 eliminate Cr(VI) in recent years. Deveci et al.¹¹ reported that coconut shell-based and
54 coal-based activated carbons were commonly used as adsorbents for Cr(VI) removal.
55 Mohan, Sarswat, Ok et al.¹² also illustrated Cr(VI) could be removed from water via
56 various adsorbents such as sugar beet tailing biochar, oak wood char and oak bark
57 char. The previous studies have illustrated that water hyacinth is a free floating
58 aquatic and recalcitrant weed which has been spread throughout the world¹³. The

59 uncontrolled growth of water hyacinth has a number of negative impacts, such as
60 interference with fishing generation, obstruction of river courses, reservoirs and water
61 channels and increasing evapo-transpiration.¹³ Therefore, the biochar derived from
62 water hyacinth following by application in the treatment of Cr(VI)-contaminated
63 water might represent an attractive pathway for removing Cr(VI) ions from water and
64 improve management of this highly problematic invasive species.¹⁴ However, biochar
65 produced directly from biomass feedstock without any pretreatment has relatively low
66 adsorption capacity. Thus, various modification/activation methods have been applied
67 to improve the adsorption performance of biochar. Previous studies have been
68 reported that several methods, such as acid and alkali modification, oxidation, and
69 chemical graft, have been used to improve their functional group contents and
70 enhance their adsorption performance.^{15, 16} However, these previous modified biochar
71 have some disadvantages: such as non-ideal adsorption capacity, occurrence of
72 secondary pollution during production, low reutilization rate and high price.¹⁷ Thus, it
73 is necessary to develop an efficient, environmentally friendly and low-cost adsorbent
74 to remove Cr(VI) from aqueous solution.

75 Nowadays, graphene oxide (GO) has attracted vast technological and scientific
76 interest due to its specific properties, such as multiple oxygen-containing functional
77 groups (hydroxyl, epoxide, carbonyl and carboxyl groups) , large specific surface
78 areas and hydrophilicity.^{18,19} At present, researchers have proved that GO could be a
79 promising material to adsorb pollutants from water, such as dyes,^{20,21} heavy metals,²²
80 polycyclic aromatic hydrocarbons (PAHs)²³ and endocrine disruptor chemicals (EDCs).

81 In addition, GO could be easily obtained from many methods^{24, 25}, which provides a
82 potential, cost-effective and large-scale production. Moreover, GO shows fine
83 biocompatibility.²⁶ Due to the above-mentioned excellent properties of graphene
84 oxide, it is believed that it could be used as coating material to functionalize various
85 adsorbent. However, GO disperses poorly in water and easily aggregates, causing its
86 surface areas to decrease and limiting its applicability. Therefore, attention has been
87 focused on integrating GO with other materials by fabricating composites to enhance
88 its applicability in the environment.²⁷ Therefore, in this work, a new composite was
89 synthesized by taking advantage of the recent methods in graphene oxide and biochar
90 technologies.

91 In this study, a novel functional adsorbent, graphene oxide coated biochar, was
92 prepared by slow pyrolysis in tube furnace at 300 °C. After systematic characterization
93 (SEM, FT-IR, XPS, BET and zeta-potential) of its structural properties, a new-type
94 resultant material was applied for removal of Cr(VI) from solution. Batch experiments
95 were carried out to study the effects of pH, ionic strength and temperature on Cr(VI)
96 adsorption. The kinetics, isotherms and thermodynamics were also utilized to evaluate
97 the adsorption properties for Cr(VI) by graphene oxide coated water hyacinth biochar
98 composite (WHB-GO). Additionally, the desorption experiment and adsorption
99 mechanism were also elucidated.

100 2. Materials and methods

101 2.1 Materials

102 All chemicals used in this work were of analytical grade, including HCl
103 (hydrochloric acid), NaOH (sodium hydroxide), H₂SO₄ (concentrated sulfuric acid),
104 KMnO₄ (potassium permanganate), NaNO₃ (sodium nitrate), H₂O₂ (hydrogen
105 peroxide), K₂S₂O₈ (potassium persulfate), P₂O₅ (phosphorus pentoxide) and K₂Cr₂O₇
106 (potassium dichromate). Synthetic graphite powder was purchased from
107 Sigma-Aldrich. Water hyacinth was collected from Ocean Lake Wetland Park of
108 Changsha, China. The materials were dried at 105 °C for 12 h and then milled into
109 powders by a high speed rotary machine prior to use.

110 2.2 Preparation of graphene oxide suspension

111 Stable graphene oxide suspension was prepared from the synthetic graphite
112 powder by using a method similar to modified Hummers method²⁸. Briefly, graphite
113 powder (3.0 g) was firstly preoxidized by concentrated H₂SO₄ (12 mL) P₂O₅ (2.5 g)
114 and K₂S₂O₈ (2.5 g) at 80 °C for 4.5 h. Then, the concentrated H₂SO₄ (120 mL),
115 KMnO₄ (15 g) and NaNO₃ (2.5 g) were used to oxidize the preoxidized graphite. After
116 that, 20 mL H₂O₂ (30 wt%) solution was added to eliminate the excess MnO₄⁻, and the
117 products were rinsed repeatedly with HCl (10%) and ultrapure water. The obtained
118 solution was sonicated for 2 h and stored in a refrigerator at 4 °C before use.

119 2.3 Preparation of adsorbent

120 The graphene oxide suspension was firstly coated on the water hyacinth powders
121 using a dip coating procedure which was similar to the previously reported.²⁹ Briefly,
122 10 g water hyacinth biomass was dipped into the graphene oxide suspension (mass
123 ratio = 1:0.06 g) and was stirred for 1 h using a magnetic stirrer at 500 rpm. After that,
124 the dip-coated GO raw materials were sonicated for 2 h to promote mix well and then
125 oven dried at 80 °C. Finally, the obtained materials were placed in tubular furnace to
126 produce the graphene oxide-coated biochar through slow pyrolysis in a N₂
127 environment at temperature of 300°C for 2 h. Untreated water hyacinth powders were
128 also used as feedstock to produce biochar without graphene oxide coating in the
129 furnace with the same pyrolysis conditions. The obtained adsorbent samples were
130 washed with ultrapure water for several times to remove impurities, then vacuum
131 dried and sealed in a desiccator for further experiment tests. The GO coated water
132 hyacinth biochar composite and pristine water hyacinth biochar were labeled as
133 WHB-GO and WHB, respectively.

134 2.4 Materials characterization

135 The scanning electron microscopy (SEM) (JSM-7001F, Japan) analysis was
136 carried out to determine the surface morphologies and microscopic features of
137 prepared materials. The Fourier transform-infrared technique (FT-IR) (Nicolet 5700
138 Spectrometer, USA) was used to determine the functional groups on the surface of
139 adsorbents before and after contacting with Cr(VI) ions. The elements of the samples

140 were performed by an ESCALAB 250Xi X-ray Photoelectron Spectrometer (XPS)
141 (Thermo Fisher, USA). The total surface areas and aperture of materials were
142 determined by the method of Brunauer, Emmett, and Teller (BET) (Tri-star 3020,
143 USA). WHB and WHB-GO samples were analyzed by BET using nitrogen as
144 adsorptive gas to characterize the surface area and total pore volume.

145 2.5 Adsorption experiment

146 A stock solution of Cr(VI) (1000 mg L^{-1}) was prepared by dissolving 2.8290 g
147 potassium dichromate ($\text{K}_2\text{Cr}_2\text{O}_7$) into 1000 mL ultrapure water. In batch experiments,
148 the different Cr(VI) concentrations were obtained by diluting the stock solution. All
149 adsorption experiments were performed in sealed 100 mL glass conical bottles that
150 contained 0.1g of WHB-GO and 50 mL of a Cr(VI) solution in an appropriate
151 concentration. The bottles were placed in a shaking water bath with a shaking speed
152 of 150 rpm for 24 h. The pH of Cr(VI) solutions was adjusted to obtain the desired
153 values by adding negligible volumes of NaOH and HCl ($0.1\text{-}0.8 \text{ mol L}^{-1}$).

154 The effect of pH on the adsorption of Cr(VI) was studied with an initial Cr(VI)
155 concentration of 100 mg L^{-1} in a pH range of 2.0 to 9.0 (2.0, 2.5, 3.0, 4.0, 5.0, 6.0, 7.0,
156 8.0 and 9.0) at $30 \text{ }^\circ\text{C}$. The zeta potentials of WHB-GO were measured in aqueous
157 solutions at pH 2.0 to 10.0 by Zetaplus 90 (Brook-haven Instruments, New York,
158 USA). The effect of the ionic strength on the adsorption of Cr(VI) was studied by
159 adding NaCl to 100 mg L^{-1} Cr(VI) solutions with concentrations ranging from 0 to 1
160 mol L^{-1} (0, 0.001, 0.005, 0.01, 0.005, 0.1, 0.5 and 1 mol L^{-1}) at $30 \text{ }^\circ\text{C}$ and pH 2.0. An

161 adsorption kinetic study was carried out with an initial Cr(VI) concentration of 100
162 mg L⁻¹ at 30 °C and pH 2.0 to determine the minimum time required for equilibrium
163 adsorption. The concentrations of Cr(VI) were measured at different time intervals
164 from 15 to 2880 min (15, 30, 60, 120, 180, 360, 480, 600, 720, 1080, 1440, 2160 and
165 2880 min). To evaluate the maximum adsorption capacity and thermodynamic
166 properties, adsorption isotherms of Cr(VI) on WHB-GO were obtained at pH 2.0 at 30
167 °C, 40 °C and 50 °C, respectively. The initial Cr(VI) concentrations ranged from 100
168 to 800 mg L⁻¹ (100, 200, 300, 400, 500, 600, 700 and 800 mg L⁻¹). Furthermore, in
169 order to better highlight the superiority of WHB-GO adsorption performance, WHB
170 and water hyacinth biomass as adsorbent were also studied. In particular, the
171 different concentrations of initial Cr(VI) solution were shaken at pH 2.0 and 30 °C.
172 The remaining concentration of Cr(VI) was determined by using a UV
173 spectrophotometer (Pgeneral T6, China) at a wavelength of 540 nm. The adsorption
174 capacity (q_e (mg g⁻¹)) and removal efficiency (E_R) of tested adsorbents at the
175 equilibrium state was calculated by the following equations:

$$176 \quad q_e = \frac{(C_0 - C_e)v}{w} \quad (1)$$

$$177 \quad E_R = \frac{C_0 - C_e}{C_0} \times 100\% \quad (2)$$

178 where v (L) is the volume of solution, w (g) is the amount of adsorbent, C_0 and C_e (mg
179 L⁻¹) are the initial and equilibrium concentrations of Cr(VI), respectively.

180 3. Result and discussion

181 3.1 Characterization of adsorbents

182 3.1.1 SEM: The surface morphologies of WHB, WHB-GO before and after
183 adsorption of Cr(VI) were displayed in the SEM images. As seen from Fig. 1(a),
184 WHB showed uneven and irregular surface, meanwhile a lot of carbon particles were
185 also observed from the surface of the pristine biochar, which indicated that the water
186 hyacinth were pyrolyzed and carbonized. However, after coating with GO, there was a
187 visible change, the WHB-GO (Fig. 1(b)) showed sheet-like structure with thick sheets
188 and wrinkled edges, which could present a higher surface area and provide effective
189 adsorption sites. After reaction with Cr(VI), the composite became much more smooth
190 and well-knit (Fig. 1(c)). This phenomenon was possibly due to the adsorption of
191 Cr(VI) onto the surface of adsorbent that blocked the pore channel.

192 3.1.2 FT-IR: The FT-IR technique was used to determine the functional groups
193 on the surface of WHB and WHB-GO (before and after adsorption) and the results
194 were presented in Fig. 2. The spectra of both WHB and WHB-GO emerged a number
195 of adsorption peaks indicating the relative complex of the materials. For the two
196 carbon materials, the characteristic peak at 3423.0 cm^{-1} was attributed to the C=O in
197 the hydroxyl groups. The bands at around 1610.3 cm^{-1} and 1319.0 cm^{-1} were assigned
198 to C-C and C-OH stretching vibration.²⁰ No obvious peak between 1200 cm^{-1} and 450
199 cm^{-1} could be found in the spectrum of WHB. Compared with the spectrum of WHB,
200 more peaks occurred in the spectra of WHB-GO. The appearance of new peaks at

201 520.7 and 470.5 cm^{-1} in the spectrum were attributed to C-H and C-O stretching
202 vibration. The new strong peaks at 1033.7 and 781.0 cm^{-1} in the spectrum of
203 WHB-GO were attributed to the stretching of C-O-C and aromatic compounds,
204 respectively.³⁰ In short, the adsorption peak of C-H, C-O, C-O-C and aromatic
205 compounds groups changed after modification, which confirmed that the surface
206 carbon functional groups of the GO were successfully introduced into the composites
207 during the pyrolysis process in the tube furnace. Therefore, the information given by
208 the FTIR spectra proves that WHB-GO was prepared successfully. Additionally, the
209 detailed description of WHB-GO loaded with Cr (WHB-GO+Cr) will be discussed in
210 the following section concerning the adsorption mechanism.

211 3.1.3 XPS: In order to gain further information on its chemical composition, XPS
212 (X-ray photoelectron spectroscopy) analysis was performed on WHB-GO before and
213 after its reaction with Cr(VI) and the results were exhibited in Fig. 3. In the XPS
214 survey, the principal elements at WHB surface were carbon (69.91%), oxygen
215 (23.86%), nitrogen (4.56%) and phosphorus (1.67%) and at WHB-GO surface were
216 carbon (66.79%), oxygen (29.55%), nitrogen (3.18%) and phosphorus (0.48%). It
217 demonstrated that the existence of carbon and oxygen composed the main body of the
218 two materials. Obviously, the ratio of carbon content to oxygen content (C/O) for
219 WHB and WHB-GO were 2.93 and 2.26, respectively, which implied that more
220 oxygen-containing functional groups, such as C=O, C-O are introduced.

221 Detailed XPS surveys of the regions for Cr_{2p} were shown in Fig. 4. The
222 high-resolution spectra of Cr-laden biomaterials indicated that there were significant

223 contributions of the Cr bound on their surfaces. The Cr_{2p} XPS spectrum of WHB-GO,
224 significant peaks centered at 575-577 and 585-588 eV were observed, which
225 corresponded to Cr 2p_{3/2} orbitals and Cr 2p_{1/2} orbitals, respectively. The Cr 2p_{3/2}
226 orbitals were assigned at 577.2 eV (CrCl₃) and 575.2–576.5 eV (Cr₂O₃) for Cr(III)
227 compounds, while Cr(VI) forms were characterized by higher binding energies such
228 as 578.1 eV (CrO₃) or 579.2 eV (K₂Cr₂O₇)³¹. As seen from the Fig.4, the binding
229 energies at 575.5 and 578.3 eV could be assigned to Cr(III) and Cr(VI), respectively³².
230 This suggested that part of adsorbed Cr(VI) anions were reduced to Cr(III) after
231 exposure to WHB-GO. Meanwhile, C1s bands and N1s bands of WHB-GO before
232 and after adsorption were also investigated. As seen from Fig. 5(a), three different
233 bands centered at 284.2eV, 285.6eV and 287.7eV were observed corresponding to C–
234 C/C=C, C–O and C=O groups of WHB-GO³³. The C 1s XPS spectrum of WHB-GO
235 loaded with Cr clearly indicated that four components corresponding to C–Cr (282.2
236 eV), C–C/C=C (284.3 eV), C–O (286.1 eV) and [Cr(CO)₆] (288.4 eV)^{34, 35}(Fig.5(b))
237 Based on the XPS results, the difference between WHB-GO and WHB-GO loaded
238 with Cr might attribute to the introduced carbon functional groups, which enhanced
239 the adsorption ability. As shown in Fig. 5(c), the N1s XPS spectrum of WHB-GO
240 composite could be curve-fitted into two band components at approximately 398.5
241 and 399.5 eV, attributable to the –N=C and N-H³⁶. After reaction with Cr(VI), a new
242 peak occurred at 401.2 eV, corresponding to nitrogen atoms in doped imine (–
243 N⁺=)³⁵(Fig.5(d)). It was probably due to the amino groups were involved in the
244 fixation of Cr(VI) and chelation of Cr(III) onto the WHB-GO. According to FT-IR

245 and XPS spectra, the GO was successfully grafted on the biochar surface, which could
246 provide more binding sites for Cr(VI) adsorption.

247 3.1.4 BET The BET (Brunauer–Emmett–Teller) surface area, pore volume and
248 average pore size of WHB and WHB-GO were displayed in Table 1. As shown in
249 Table 1, the BET surface area of WHB-GO ($25.89 \text{ m}^2 \text{ g}^{-1}$) was larger than that of
250 WHB ($8.85 \text{ m}^2 \text{ g}^{-1}$), which could explain that the GO was successfully grafted on
251 WHB and increased the surface area of WHB-GO. However, WHB-GO possessed
252 smaller pore volume and pore size than WHB. The phenomenon might be attributed to
253 the process of preparing WHB-GO, in which water hyacinth biomass was immersed
254 into graphene oxide solution and changed the pore structure of WHB. Besides, the
255 ratio change of some functional groups might constrain N_2 in some pore networks and
256 thus the pore volume distribution changed.

257 3.2 Effect of pH on Cr (VI) adsorption

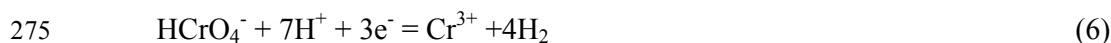
258 Solution pH is a significant controlling factor in sorption process. In order to
259 determine the effect of pH on Cr(VI) removal by the WHB-GO, batch adsorption
260 experiments were conducted. Results (Fig. 6) showed that pH ranged from 2.0 to 9.0,
261 the Cr(VI) and total Cr sorption capacities reduced sharply and the maximum
262 adsorption capacity of Cr(VI) was obtained at pH 2.0. Therefore, it was concluded
263 that acidic condition might be more favorable for the Cr(VI) removal by the
264 WHB-GO.

265 The hexavalent chromium existed in different forms in aqueous solutions at

266 different pH values and Cr(VI) concentrations, such as H_2CrO_4 (at pH less than about
267 1.0), HCrO_4^- (at pH between 1.0 and 6.0) and CrO_4^{2-} (at pH above 6.0).³⁷



271 In other words, the Cr(VI) ions existed mainly in the form of an anion. Fig. 6
272 illustrated that the adsorption capacity of hexavalent chromium in the solution was
273 lower than total chromium. It was suggested that a part of toxic Cr(VI) might be
274 reduced to the Cr(III) according to the following electron transfer reactions:



277 The zeta potentials of WHB-GO at different pH values were shown in Fig. 7. As
278 shown in Fig. 7, the zeta potential of WHB-GO decreased with the increasing of pH
279 and the zero point of zeta potential (pH_{pzc}) was obtained at pH 2.1. At $\text{pH} < 2.1$, the
280 zeta potentials of WHB-GO are positive. At $\text{pH} > 2.1$, the surfaces of WHB-GO are
281 negatively charged. At low pH, the high adsorption capacity could be attributed to the
282 strong electrostatic attraction between the positively charged adsorbent surfaces and
283 the negatively charged chromate ions.³⁸ With increasing of pH value, the buildup of
284 negative charge on the WHB-GO surfaces resulted in electrostatic repulsion between
285 Cr(VI) ions and the sorbents, which consequently reduced the Cr(VI) sorption.³⁹
286 Besides, in high pH solution, the excessive OH^- could compete with Cr(VI) ions for
287 the available adsorption sites on the surface of WHB-GO. Therefore, the initial

288 solution pH 2.0 was used as the optimum pH for the further experiments.

289 3.3 Effect of ionic strength on Cr(VI) adsorption

290 Ionic strength is a very important variable affecting the adsorption of heavy
291 metal ions at aqueous solutions⁴⁰. To investigate the effect of ionic strength on Cr(VI)
292 adsorption, batch experiments at different concentrations of NaCl was conducted. As
293 seen from Fig. 8, the adsorption capacity of Cr(VI) on WHB-GO decreased with the
294 increasing of NaCl concentration from 0.001 to 1 mol L⁻¹, which might attribute to the
295 following three possible reasons: (1) Cl⁻ and Na⁺ were monovalent ions, they could
296 only slightly compete for the adsorption site of WHB-GO at low concentrations; (2)
297 With the increase concentration of NaCl, the screening effect increased between the
298 negatively charged Cr(VI) in solution and the positively charged adsorbent surface;⁴¹
299 (3) High concentration of NaCl improved the ionic strength of the solution which led
300 to decrease in the number of collisions between Cr(VI) ions and WHB-GO.⁴²

301 3.4 Adsorption kinetics

302 In order to study the effect of the contact time on adsorption of Cr(VI) by
303 WHB-GO, the adsorption kinetics experiments were carried out. As shown in Fig.
304 9(a), the removal capacity of Cr(VI) by WHB-GO increased rapidly in the first 6 h,
305 which might due to the abundant availability of active binding sites on the adsorbent
306 surface. And then, the adsorption rate of Cr(VI) became slower and continued a long
307 period of time until sorption equilibrium was attained at 24 h. The slow adsorption

308 process might be explained that the majority of active surface sites were occupied by
309 Cr(VI) ions and there were insufficient binding sites for Cr(VI) to use.

310 In this research, two mathematical models (pseudo-first-order and
311 pseudo-second-order models) were used to investigate the mechanism of the
312 adsorption process. The equations are generally expressed as follows:¹

$$313 \quad \ln(q_e - q_t) = \ln q_e - k_1 t \quad (8)$$

$$314 \quad \frac{t}{q_t} = \frac{1}{k_2 q_e^2} + \frac{t}{q_e} \quad (9)$$

315 where q_e and q_t (mg g^{-1}) are the adsorption amounts at equilibrium and at any time t ,
316 respectively, k_1 (min^{-1}) is the pseudo-first-order reacted rate constant, k_2 ($\text{g mg}^{-1} \text{min}^{-1}$)
317 is the pseudo-second-order reacted rate constant.

318 The kinetic parameters for Cr(VI) adsorption were calculated by the two models.
319 As can be seen from the Table 2, the correlation coefficients (R^2) of the
320 pseudo-first-order and pseudo-second-order equations were 0.92 and 0.99,
321 respectively. What's more, the calculated q_e values (48.84 mg g^{-1}) of the
322 pseudo-second-order model were more agreeable to the experimental data than the
323 values of pseudo-fist-order model. These results indicated that the
324 pseudo-second-order kinetic model could better fit the adsorption process Therefore,
325 the mechanism of Cr(VI) sorption by WHB-GO could be the chemical interaction,
326 such as complexation and redox reaction.

327 3.5 Adsorption isotherms

328 It is important to study the equilibrium adsorption isotherms, since it can provide

329 detailed information to further discuss the adsorption mechanism. In this paper,
330 Langmuir and Freundlich adsorption models were used to simulate the adsorption
331 isotherms data. The Langmuir model assumes monolayer adsorption onto a
332 homogeneous surface with no interactions between the adsorbed molecules. However,
333 the Freundlich models are empirical equations, which are often used to describe the
334 adsorption on a heterogeneous surface without saturation of adsorbent binding sites.
335 The two adsorption models were expressed by the following equations:

$$336 \quad \frac{C_e}{q_e} = \frac{1}{q_{\max}K_L} + \frac{C_e}{q_{\max}} \quad (10)$$

$$337 \quad \ln q_e = \ln K_F + 1/n \ln C_e \quad (11)$$

338 where C_e and q_e (mg g^{-1}) represent the equilibrium concentration and the adsorption
339 capacity at equilibrium, respectively, q_{\max} (mg g^{-1}) is the maximum adsorption
340 capacity, K_L (L mg^{-1}) is the Langmuir constant related to the affinity of the binding
341 sites, K_F (mg g^{-1}) is the Freundlich adsorption coefficient and n is an index of isotherm
342 nonlinearity which is related to the adsorption capacity and intensity.

343 Fig. 10 showed the plots of Langmuir and Freundlich adsorption isotherms of the
344 Cr(VI) on WHB-GO at three different temperatures and the adsorption coefficients
345 were listed in Table 3. As can be seen from the Fig. 10, the adsorption capacity
346 increased with the increase of temperature. The maximum adsorption amount was
347 approximate 150.02 mg g^{-1} , which was obtained at the temperature of $50 \text{ }^\circ\text{C}$. Table 3
348 showed that the correlation coefficient (R^2) values of Freundlich model (0.98, 0.98
349 and 0.98) at three temperatures were much better than those of Langmuir model (0.95,
350 0.94 and 0.90). Therefore, compared to the Langmuir model, the experimental data

351 were much more suitable for the Freundlich model within the studied temperature
352 range, which suggested that the adsorption of Cr(VI) onto the adsorbent was mainly
353 controlled by the Freundlich surface adsorption mechanisms. The Freundlich model
354 constant n values were range from 4.52 to 5.75, which indicated that the adsorption
355 between metal ions and adsorbent was favorable. The larger value of n could be
356 explained by stronger interaction between adsorbent and heavy metal.⁴³

357 3.6 Adsorption thermodynamic studies

358 To further study the effect of temperature on the adsorption of Cr(VI) ions onto
359 WHB-GO, thermodynamic parameters including Gibbs free energy change (ΔG°),
360 enthalpy change (ΔH°), and entropy change (ΔS°) were calculated by following
361 equations:

$$362 \quad \Delta G^\circ = -RT \ln K^\circ \quad (12)$$

$$363 \quad \ln K^\circ = \frac{\Delta S^\circ}{R} - \frac{\Delta H^\circ}{RT} \quad (13)$$

364 where R (8.314 J mol⁻¹ K⁻¹) is the universal gas constant, T (K) is the absolute
365 temperature in Kelvin, K° can be calculated by plotting $\ln K_d$ ($K_d = q_e/C_e$) versus C_e
366 and extrapolating C_e to zero, The values of ΔS° and ΔH° can be obtained from the
367 intercept and slope of the $\ln K^\circ$ against $1/T$ (Fig. 11) respectively.

368 The results on the effect of temperature indicated that the maximum adsorption
369 of Cr(VI) was obtained at 50 °C, and the maximum adsorption capacity ranged from
370 127.06 mg g⁻¹ to 150.02 mg g⁻¹ as the temperature increased from 30 °C to 50 °C. The
371 calculated results of thermodynamic parameters for the adsorption of Cr(VI) on

372 WHB-GO were shown in Table 4. As can be seen, the negative values of ΔG°
373 decrease from -2.239 to -5.148 kJ mol⁻¹ with the increase of temperature in the range
374 of 30-50 °C. This phenomenon suggested that the Cr(VI) adsorption process was
375 spontaneous and became more favorable at higher temperatures. The standard changes
376 enthalpy (ΔH°) of the adsorption process was 31.265 kJ mol⁻¹, which verified that the
377 adsorption of Cr(VI) ions using the WHB-GO was endothermic in nature. The
378 positive value of ΔS° suggested that an increased randomness occurred at the solid
379 solution interface during the adsorption process.⁴⁴ In short, the sorption process of
380 Cr(VI) onto WHB-GO was endothermic and spontaneous.

381 3.7 Comparison experiments

382 In order to highlight the superiority of WHB-GO, the comparison experiments of
383 removal efficiency by WHB and water hyacinth biomass were also conducted. As
384 seen from the Fig. 12, the Cr(VI) removal efficiency of the WHB-GO ranged from
385 95.6% to 34.9%, while the WHB and water hyacinth biomass changed from 72.3% to
386 24.9% and 48.8% to 14.2%, respectively. Obviously, the removal efficiency of Cr(VI)
387 by the WHB-GO was much higher than WHB and water hyacinth biomass. The high
388 adsorption capacity and removal efficiency of the WHB-GO could be attributed to the
389 introduction of GO molecules, which increased surface areas and multiple functional
390 groups of the adsorbent. A comparison has also been made between the resultant
391 WHB-GO and previously reported adsorbents for maximum Cr(VI) adsorption
392 (Table.5). The results of the analyses demonstrated that this novel functional

393 adsorbent gained advantage over many other adsorbents. It indicated that WHB-GO
394 was a fairly promising candidate for the treatment of chromium-containing
395 wastewater.

396 3.8 Mechanisms of Cr(VI) removal by WHB-GO

397 As discussed in the effect of pH on Cr(VI) adsorption, the electrostatic attraction
398 is regarded as a adsorption force. However, various types of interactions may also
399 involve in the adsorption process. To verify the adsorption mechanism, the FT-IR
400 spectrums (Fig. 2) and XPS (Fig.5) of Cr loaded WHB-GO were investigated. The
401 FT-IR spectra corresponding to the WHB-GO loaded with Cr(VI) exhibited an
402 apparent shift in the bending mode at 1610.3 cm^{-1} (C=C) and 781.0 cm^{-1} (aromatic
403 compounds) and the peak of 1319.0 cm^{-1} (C-OH) disappeared. The results indicated
404 that the mechanism of Cr(VI) adsorption onto WHB-GO might rely on the functional
405 groups (C=C, aromatic compounds and C=O) on the material surface. Based on XPS,
406 both Cr(VI) and Cr(III) peaks (Fig. 4) were observed, which implied that the
407 adsorption process involved the reduction of Cr(VI) into Cr(III) with its subsequent
408 partial sorption.

409 According to the above results, we hypothesized that the adsorption mechanism
410 of Cr(VI) ions by WHB-GO via electrostatic attraction of Cr(VI) coupled with Cr(VI)
411 reduction to Cr(III) and Cr(III) complexation.⁴⁵ The various mechanisms proposed for
412 the interaction of adsorbent with Cr(VI) were summarized in Fig. 13. Especially,
413 under strongly acidic environment, the removal rate of Cr(VI) in the aqueous phase

414 was faster since the negatively charged Cr(VI) species were migrated to the positively
415 surface of WHB-GO (protonated hydroxyl groups and carbonyl groups) with the help
416 of electrostatic driving forces. While, both direct and/or indirect reduction
417 mechanism(s) involved during the adsorption process. In direct reduction process,
418 Cr(VI) was directly reduced to Cr(III) in the aqueous phase by contact with
419 electron-donor groups of WHB-GO and the reduced-Cr(III) remained in the aqueous
420 solution or formed complexes with Cr-binding groups of it. Indirect reduction
421 mechanism consisted of three steps: (1) the binding of anionic Cr(VI) to positively
422 charged groups present on the surface of WHB-GO; (2) the reduction of Cr(VI) into
423 Cr(III) by adjacent electron-donor groups³¹ and (3) the partial release of the
424 reduced-Cr(III) into the aqueous phase due to electronic repulsion between the
425 positively-charged groups and the Cr(III), or complexation of the reduced-Cr(III) with
426 rest functional groups on the WHB-GO. On the basis of the above analyses, amine,
427 hydroxyl and carbonyl groups could be the main functional groups for Cr(VI)
428 sorption.

429 3.9 Regeneration of WHB-GO

430 In order to assess the practical utility of the WHB-GO adsorbent, adsorption–
431 desorption experiments were conducted by using 0.5mol L⁻¹ sodium hydroxide and
432 the results were shown in Fig. 14. The results demonstrated that the adsorption
433 activity of WHB-GO only slightly decreased with increasing the number of reuse
434 cycles. The adsorption capacity could still reach 69.10 mg g⁻¹ on the sixth reuse cycle,

435 which only reduced by 7.43% compared to that of the first cycle. The excellent
436 regeneration performance indicated that the WHB-GO could be a cost-effective,
437 efficient and potential adsorbent for Cr(VI) removal. In short, the WHB-GO not only
438 had a high adsorption capability, but also possessed a stable performance during the
439 cycles.

440 **4. Conclusions**

441 In this work, a new low cost adsorbent was successfully synthesized and applied
442 to remove Cr(VI) from aqueous solution. Results showed that the modification
443 significantly improved the adsorption performance for Cr(VI) removal by combining
444 its adsorption and reduction dual functions. The adsorption capacity was significantly
445 affected by the solution pH and the maximum Cr(VI) adsorption capacity (150.02mg
446 g⁻¹) was obtained at pH 2.0. Background ionic strength exerted obvious influence on
447 the Cr(VI) uptake at the high concentrations of NaCl solution. The experimental data
448 were better fitted by the pseudo-second-order and Freundlich models.
449 Thermodynamic evaluation revealed that the adsorption process was spontaneous and
450 endothermic. Besides, the adsorbent had a good stability during the adsorption–
451 desorption cycles without significant reduction of the adsorption capacity. The results
452 indicated that the new engineered composite can be an innovative and alternative
453 adsorbent, which can effectively and economically remove Cr(VI) ions from aqueous
454 solution.

455 **Acknowledgments**

456 The authors gratefully acknowledge financial support from the National Natural
457 Science Foundation of China (Grant no. 41271332 and 51478470) and the Hunan
458 Provincial Innovation Foundation for Postgraduate (Grant No. CX2015B090).

References

1. C. Gan, Y. Liu, X. Tan, S. Wang, G. Zeng, B. Zheng, T. Li, Z. Jiang and W. Liu, *RSC Adv.*, 2015, **5**, 35107-35115.
2. J. J. Pan, J. Jiang and R. K. Xu, *Chemosphere*, 2014, **101**, 71-76.
3. L. Tang, G.-D. Yang, G.-M. Zeng, Y. Cai, S.-S. Li, Y.-Y. Zhou, Y. Pang, Y.-Y. Liu, Y. Zhang and B. Luna, *Chemical Engineering Journal*, 2014, **239**, 114-122.
4. N. Adhoum, L. Monser, N. Bellakhal and J. E. Belgaied, *J Hazard Mater*, 2004, **112**, 207-213.
5. A. Hafez and S. El-Mariharawy, *Desalination*, 2004, **165**, 141-151.
6. S. Rengaraj, C. K. Joo, Y. Kim and J. Yi, *Journal of Hazardous Materials*, 2003, **102**, 257-275.
7. Y. Pang, G. M. Zeng, L. Tang, Y. Zhang, Y. Y. Liu, X. X. Lei, M. S. Wu, Z. Li and C. Liu, *Bioresour Technol*, 2011, **102**, 10733-10736.
8. S. Luo, X. Xu, G. Zhou, C. Liu, Y. Tang and Y. Liu, *J Hazard Mater*, 2014, **274**, 145-155.
9. Y. Wu, H. Luo, H. Wang, C. Wang, J. Zhang and Z. Zhang, *J Colloid Interface Sci*, 2013, **394**, 183-191.
10. S. A. Baig, J. Zhu, N. Muhammad, T. Sheng and X. Xu, *Biomass and Bioenergy*, 2014, **71**, 299-310.
11. H. Deveci and Y. Kar, *Journal of Industrial and Engineering Chemistry*, 2013, **19**, 190-196.
12. D. Mohan, A. Sarswat, Y. S. Ok and C. U. Pittman, Jr., *Bioresour Technol*, 2014, **160**, 191-202.
13. Z. Hu, X. Ma and L. Li, *Energy Conversion and Management*, 2015, **94**, 337-344.
14. M.-m. Zhang, Y.-g. Liu, T.-t. Li, W.-h. Xu, B.-h. Zheng, X.-f. Tan, H. Wang, Y.-m. Guo, F.-y. Guo and S.-f. Wang, *RSC Adv.*, 2015, **5**, 46955-46964.
15. Z. Li, T. Katsumi, T. Inui and S. Imaizumi, *Adsorption Science & Technology*, 2010, **28**, 419-435.
16. P. Liu, W. J. Liu, H. Jiang, J. J. Chen, W. W. Li and H. Q. Yu, *Bioresour Technol*, 2012, **121**, 235-240.
17. Y. Feng, H. Zhou, G. Liu, J. Qiao, J. Wang, H. Lu, L. Yang and Y. Wu, *Bioresour Technol*, 2012, **125**, 138-144.
18. H. Wang, X. Yuan, Y. Wu, H. Huang, X. Peng, G. Zeng, H. Zhong, J. Liang and M. Ren, *Adv Colloid Interface Sci*, 2013, **195-196**, 19-40.
19. J. Xu, L. Wang and Y. Zhu, *Langmuir*, 2012, **28**, 8418-8425.
20. O. Moradi, V. K. Gupta, S. Agarwal, I. Tyagi, M. Asif, A. S. H. Makhlof, H. Sadegh and R. Shahryari-ghoshekandi, *Journal of Industrial and Engineering Chemistry*, 2015, **28**, 294-301.
21. J. Z. Sun, Z. H. Liao, R. W. Si, G. P. Kingori, F. X. Chang, L. Gao, Y. Shen, X. Xiao, X. Y. Wu and Y. C. Yong, *Water Sci Technol*, 2014, **70**, 1663-1669.
22. S. R, T. E, Z. B, M. E, T. E, H. J, G. A, F. B and W. R, *Dalton Transactions*, 2013, **42**, 5682-5689.
23. J. Wang, Z. Chen and B. Chen, *Environmental science & technology*, 2014, **48**, 4817-4825.
24. H. Wang, Y.-g. Liu, G.-m. Zeng, X.-j. Hu, X. Hu, T.-t. Li, H.-y. Li, Y.-q. Wang and L.-h.

- Jiang, *Carbohydrate polymers*, 2014, **113**, 166-173.
25. P. Avouris and C. Dimitrakopoulos, *Materials today*, 2012, **15**, 86-97.
26. H. Yan, X. Tao, Z. Yang, K. Li, H. Yang, A. Li and R. Cheng, *J Hazard Mater*, 2014, **268**, 191-198.
27. J. Liu, G. Liu and W. Liu, *Chemical Engineering Journal*, 2014, **257**, 299-308.
28. Z. Wu, H. Zhong, X. Yuan, H. Wang, L. Wang, X. Chen, G. Zeng and Y. Wu, *Water Res*, 2014, **67**, 330-344.
29. M. Inyang, B. Gao, A. Zimmerman, Y. Zhou and X. Cao, *Environ Sci Pollut Res Int*, 2015, **22**, 1868-1876.
30. J. Ma, P. Cai, W. Qi, D. Kong and H. Wang, *Colloids and Surfaces A: Physicochemical and Engineering Aspects*, 2013, **426**, 6-11.
31. D. Park, S. R. Lim, Y. S. Yun and J. M. Park, *Bioresour Technol*, 2008, **99**, 8810-8818.
32. H. Cui, M. Fu, S. Yu and M. K. Wang, *J Hazard Mater*, 2011, **186**, 1625-1631.
33. J. N. Tiwari, K. Mahesh, N. H. Le, K. C. Kemp, R. Timilsina, R. N. Tiwari and K. S. Kim, *Carbon*, 2013, **56**, 173-182.
34. W. Xu, S. Wang, Y. Liu, G. Zeng, B. Zheng, X. Tan, T. Li, H. Wang, F. Guo and M. Zhang, *RSC Adv.*, 2015, **5**, 24009-24015.
35. G. Yang, L. Tang, Y. Cai, G. Zeng, P. Guo, G. Chen, Y. Zhou, J. Tang, J. Chen and W. Xiong, *RSC Adv.*, 2014, **4**, 58362-58371.
36. G. X. Yang and H. Jiang, *Water Res*, 2014, **48**, 396-405.
37. D. Mohan and C. U. Pittman, Jr., *J Hazard Mater*, 2007, **142**, 1-53.
38. M. QuiIntana, G. Curutchet and E. Donati, *Biochemical Engineering Journal*, 2001, **9**, 11-15.
39. X. Dong, L. Q. Ma and Y. Li, *J Hazard Mater*, 2011, **190**, 909-915.
40. T. S. Anirudhan and M. Ramachandran, *Ind.eng.chem.res*, 2008, **47**.
41. F.-y. Guo, Y.-g. Liu, H. Wang, G.-m. Zeng, X.-j. Hu, B.-h. Zheng, T.-t. Li, X.-f. Tan, S.-f. Wang and M.-m. Zhang, *RSC Adv.*, 2015, **5**, 45384-45392.
42. Z.-b. Zhang, X.-h. Cao, P. Liang and Y.-h. Liu, *Journal of Radioanalytical and Nuclear Chemistry*, 2012, **295**, 1201-1208.
43. M. Lu, Y.-g. Liu, X.-j. Hu, Y. Ben, X.-x. Zeng, T.-t. Li and H. Wang, *Journal of Central South University*, 2013, **20**, 2478-2488.
44. G. Zhao, J. Li and X. Wang, *Chemical Engineering Journal*, 2011, **173**, 185-190.
45. D. Park, Y. S. Yun, J. H. Jo and J. M. Park, *Water Res*, 2005, **39**, 533-540.

Figure captions

Fig. 1 SEM images of WHB (a), WHB-GO (b), and after adsorption of Cr(VI) on WHB-GO (c)

Fig. 2 FT-IR spectra of WHB, WHB-GO and adsorption of Cr(VI) on WHB-GO (WHB-GO+Cr).

Fig. 3 XPS survey spectra of WHB and WHB-GO before and after adsorption (WHB-GO+Cr).

Fig. 4 The Cr2p XPS spectra of WHB-GO

Fig. 5 The C1s XPS spectra of WHB-GO before (a) and after adsorption (b); the N1s XPS spectra of WHB-GO before (c) and after adsorption (d)

Fig. 6 Effect of initial solution pH values on Cr(VI) and total Cr removal by WHB-GO (Cr(VI) solution volume: 50 mL; adsorbent dose: 0.1 g; contact time: 24 h; initial Cr(VI) concentration: 100 mg L⁻¹).

Fig. 7 Zeta potentials of WHB-GO at different solution pH (Cr(VI) solution volume: 50 mL; adsorbent dose: 0.1 g; contact time: 24 h; initial Cr(VI) concentration: 100 mg L⁻¹).

Fig. 8 Effect of different concentrations of NaCl on Cr(VI) removal by WHB-GO (volume: 50 mL; adsorbent dose: 0.1 g; initial Cr(VI) concentration: 100 mg L⁻¹; pH: 2.0; contact time: 24 h).

Fig. 9 Kinetics of Cr(VI) adsorption onto the WHB-GO at 30 °C (initial Cr(VI) concentration 100 mg L⁻¹; pH:2.0). (a) Cr(VI) sorption kinetics data; (b) pseudo-second-order model for Cr(VI) adsorption

Fig. 10 Langmuir and Freundlich isotherms of Cr(VI) adsorption on WHB-GO (Cr(VI) solution volume: 50 mL; adsorbent dose: 0.1 g; contact time: 24 h; pH: 2.0).

Fig. 11 Plot of $\ln k^0$ versus $1/T$ for estimation of thermodynamic parameters for the adsorption of Cr(VI) on WHB-GO (volume: 50 mL; adsorbent dose: 0.1 g; initial Cr(VI) concentration: 100, 200, 300, 400, 500, 600, 700 and 800 mg L⁻¹; pH: 2.0; contact time: 24 h).

Fig. 12 The comparison of Cr(VI) removal efficiency among the WHB-GO, WHB and WH biomass (Cr(VI) solution volume: 50 mL; adsorbent dose: 0.1 g; contact time: 24 h; pH: 2.0).

Fig.13 The schematic illustration of Cr(VI) sorption mechanisms on WHB-GO

Fig. 14 Sixth consecutive adsorption–desorption cycles of WHB-GO for Cr(VI) removal (volume: 50 mL; adsorbent dose: 0.1 g; initial Cr(VI) concentration: 200 mg L⁻¹; pH: 2.0; contact time: 24 h)

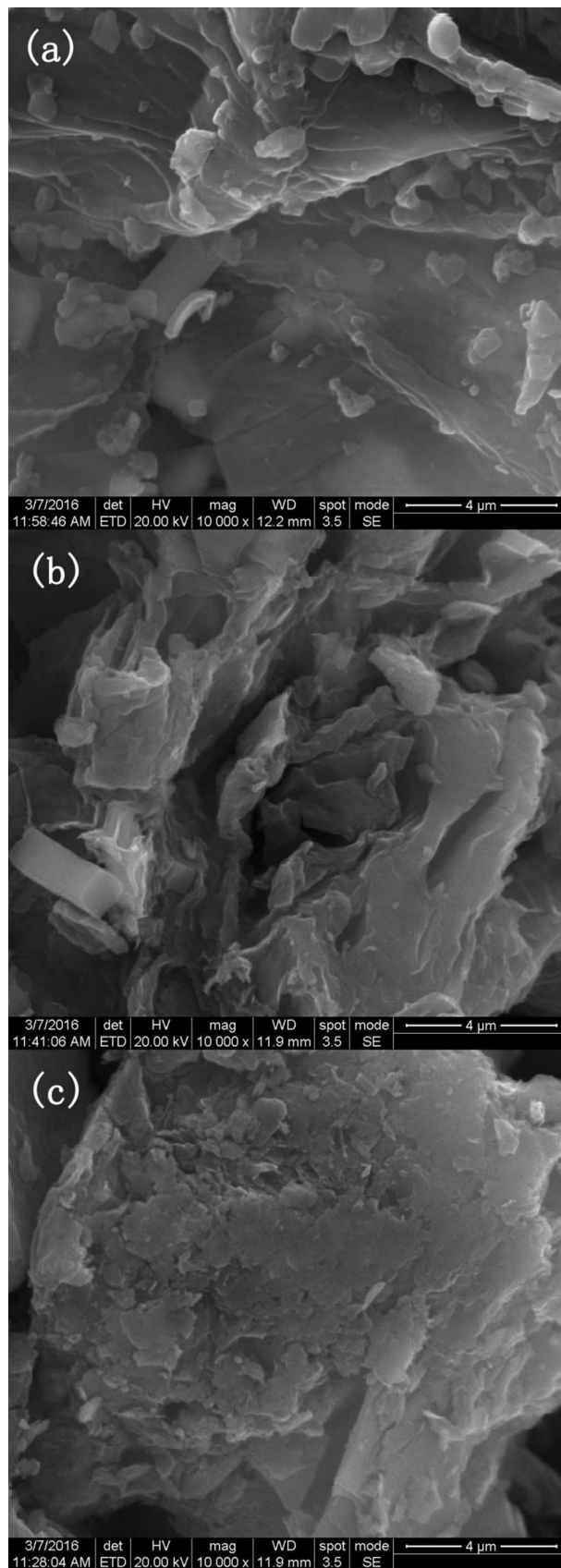


Fig. 1 SEM images of WHB (a), WHB-GO (b), and after adsorption of Cr(VI) on WHB-GO (c) (WHB-GO+Cr).

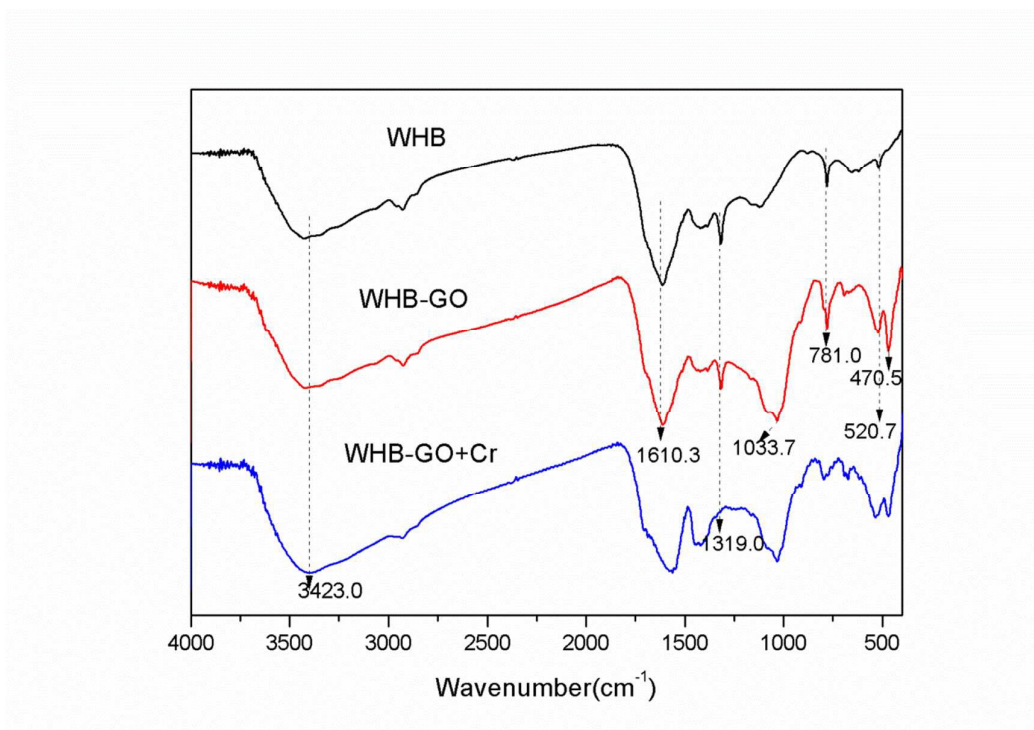


Fig. 2 FT-IR spectra of WHB, WHB-GO and adsorption of Cr(VI) on WHB-GO (WHB-GO+Cr).

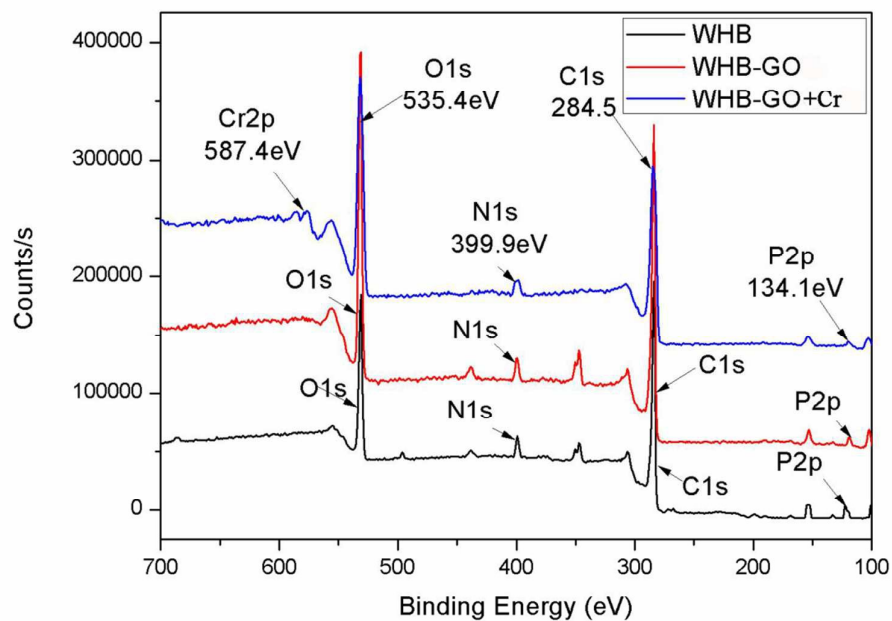


Fig. 3 XPS survey spectra of WHB and WHB-GO before and after adsorption (WHB-GO+Cr)

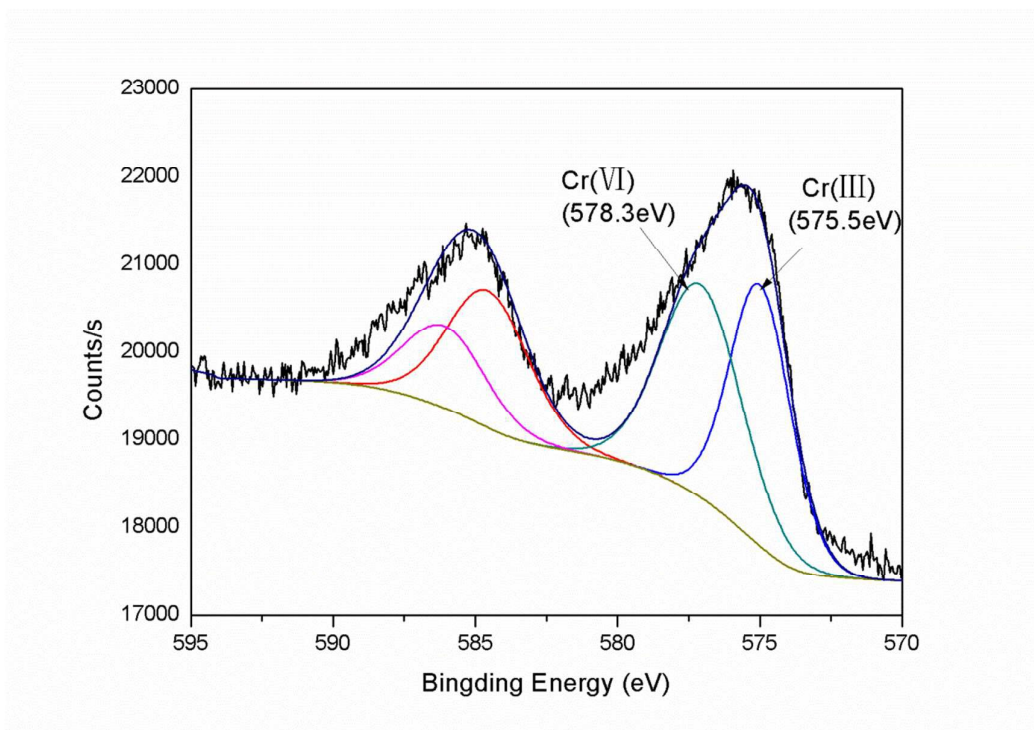


Fig. 4 The Cr_{2p} XPS spectra of WHB-GO

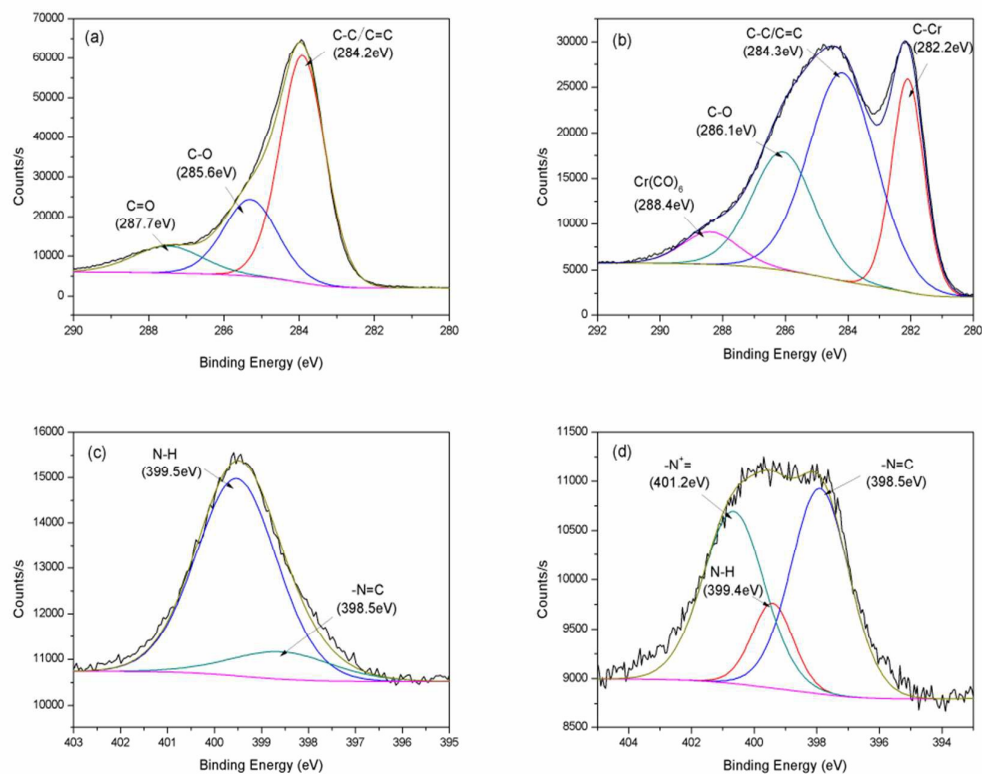


Fig. 5 The C1s XPS spectra of WHB-GO before (a) and after adsorption (b); the N1s XPS spectra of WHB-GO before (c) and after adsorption (d)

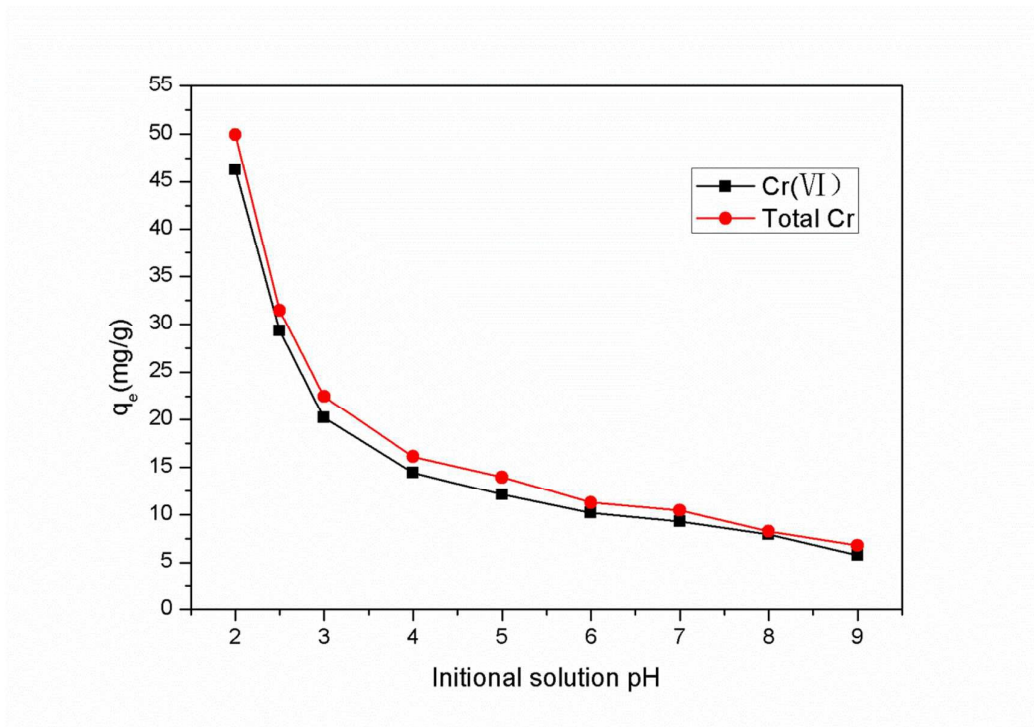


Fig. 6 Effect of initial solution pH values on Cr(VI) and total Cr removal by WHB-GO (Cr(VI) solution volume: 50 mL; adsorbent dose: 0.1 g; contact time: 24 h; initial Cr(VI) concentration: 100 mg L⁻¹).

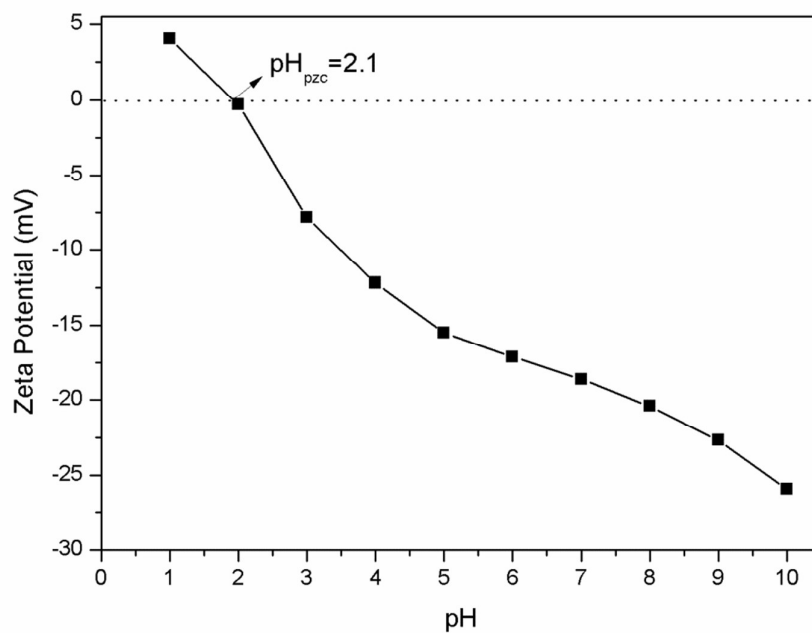


Fig. 7 Zeta potentials of WHB-GO at different solution pH (Cr(VI) solution volume: 50 mL; adsorbent dose: 0.1 g; contact time: 24 h; initial Cr(VI) concentration: 100 mg L⁻¹).

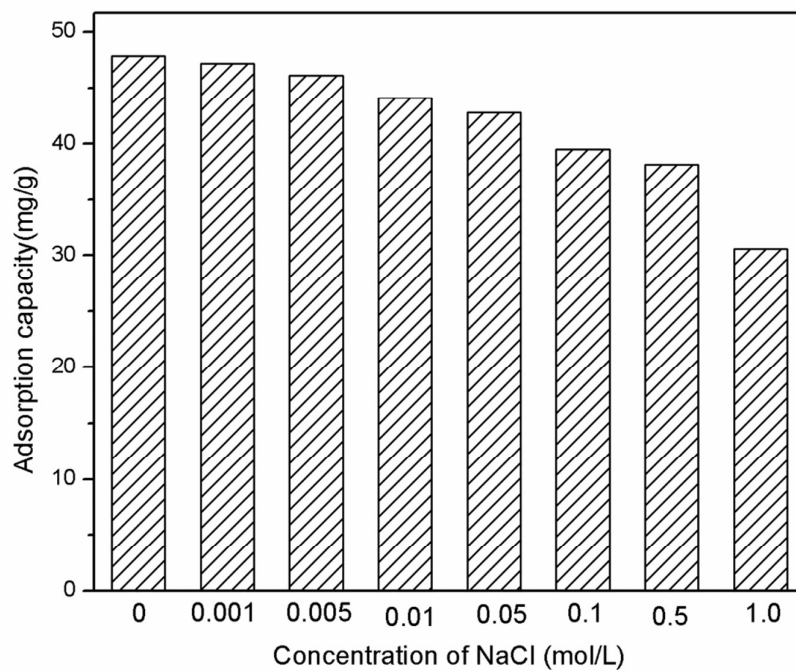


Fig. 8 Effect of different concentrations of NaCl on Cr(VI) removal by WHB-GO (volume: 50 mL; adsorbent dose: 0.1 g; initial Cr(VI) concentration: 100 mg L⁻¹; pH: 2.0; contact time: 24 h).

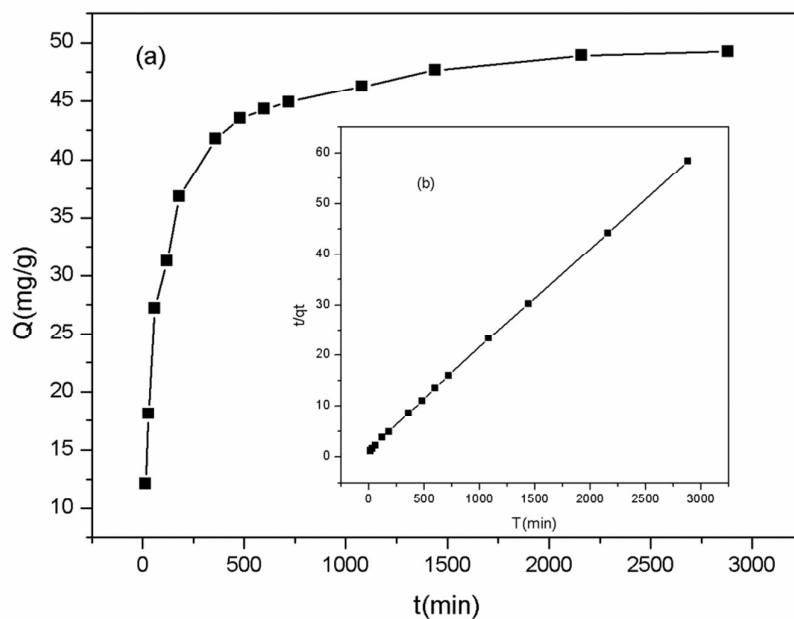


Fig. 9 Kinetics of Cr(VI) adsorption onto the WHB-GO at 30°C (initial Cr(VI) concentration 100 mgL⁻¹; pH:2.0). (a) Cr(VI) sorption kinetics data; (b) pseudo-second-order model for Cr(VI) adsorption.

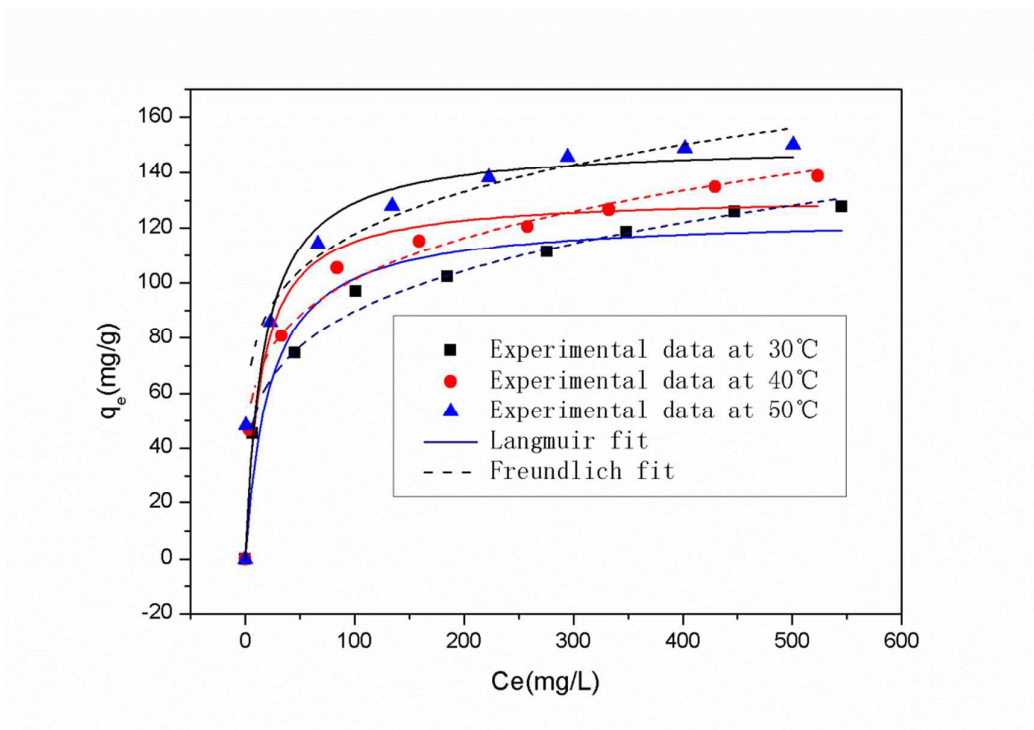


Fig. 10 Langmuir and Freundlich isotherms of Cr(VI) adsorption on WHB-GO (Cr(VI) solution volume: 50 mL; adsorbent dose: 0.1 g; contact time: 24 h; pH: 2.0).

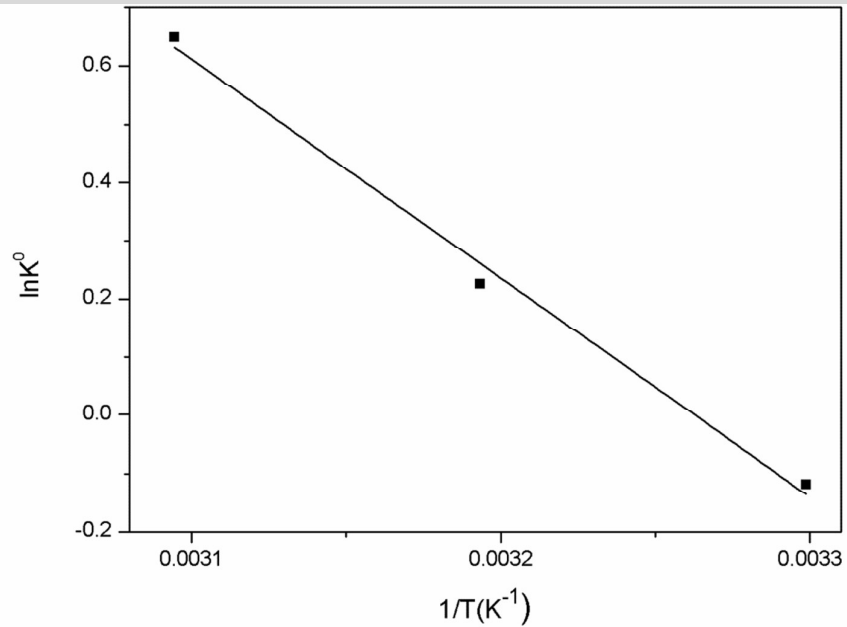


Fig. 11 Plot of $\ln k^0$ versus $1/T$ for estimation of thermodynamic parameters for the adsorption of Cr(VI) on WHB-GO (volume: 50 mL; adsorbent dose: 0.1 g; initial Cr(VI) concentration: 100, 200, 300, 400, 500, 600, 700 and 800 mg L⁻¹; pH: 2.0; contact time: 24 h).

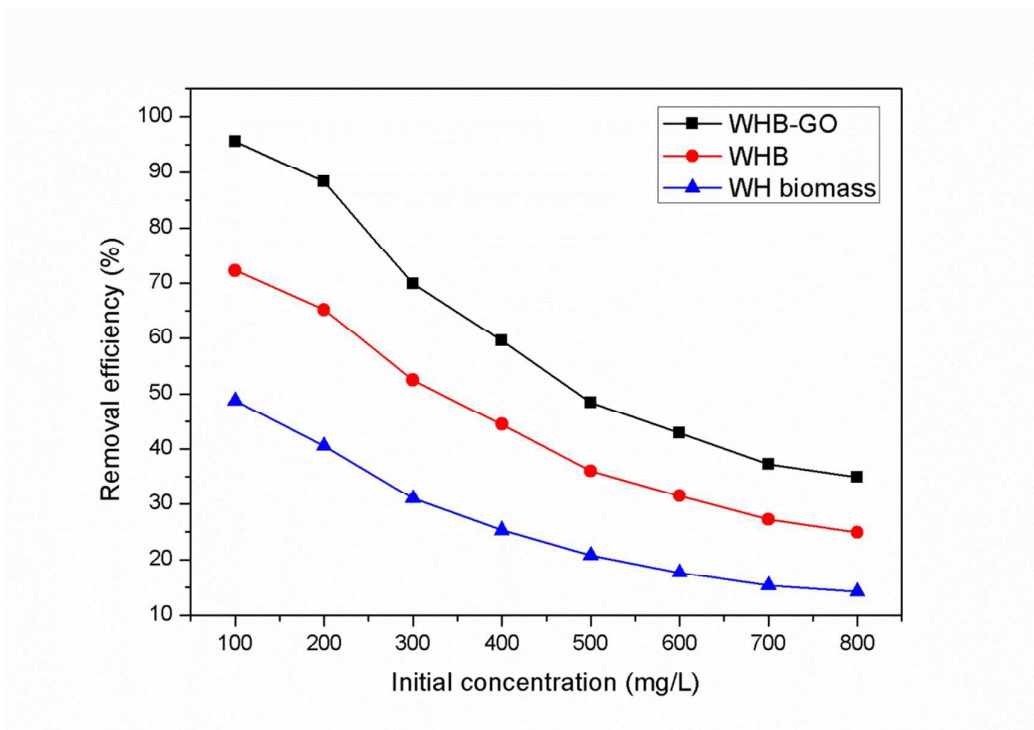


Fig. 12 The comparison of Cr(VI) removal efficiency among the WHB-GO, WHB and WH biomass (Cr(VI) solution volume: 50 mL; adsorbent dose: 0.1 g; contact time: 24 h; pH: 2.0).

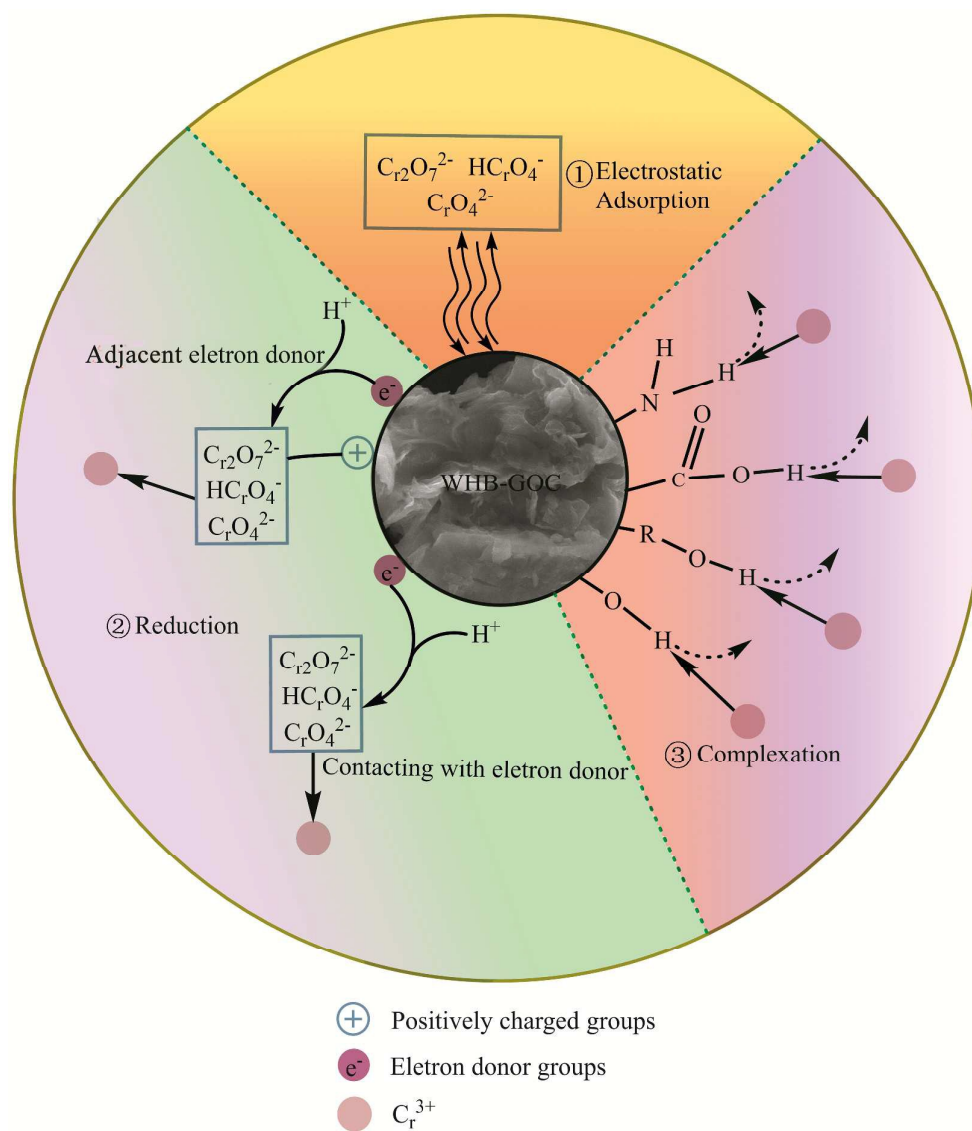


Fig.13 The schematic illustration of Cr(VI) sorption mechanisms on WHB-GO

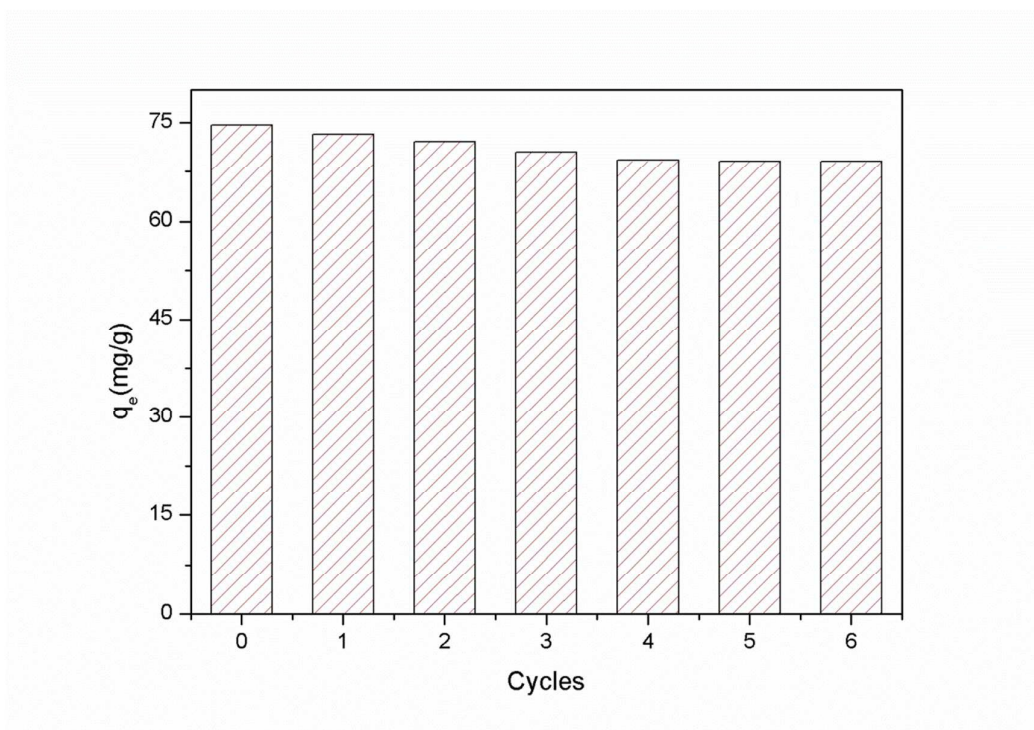


Fig. 14 Sixth consecutive adsorption–desorption cycles of WHB-GO for Cr(VI) removal (volume: 50 mL; adsorbent dose: 0.1 g; initial Cr(VI) concentration: 200 mg L⁻¹; pH: 2.0; contact time: 24 h)

Tables

Table 1 Selected physical properties of pristine biochar and WHB-GO.

Adsorbent	BET surface area (cm ² g ⁻¹)	Pore volume (cm ³ g ⁻¹)	Pore size (nm)
WHB	8.85	0.025	1.716
WHB-GO	25.89	0.019	1.613

Table 2 Pseudo-first-order model and pseudo-second-order model parameters for Cr(VI) adsorption on WHB-GO.

Pseudo-first-order		Model	Pseudo-second-order		model
K_1	q_e		K_2	q_e	
(min^{-1})	(mg g^{-1})	R^2	($\text{g mg}^{-1} \text{min}^{-1}$)	(mg g^{-1})	R^2
0.013	45.41	0.92	3.8×10^{-4}	48.84	0.99

Table 3 Langmuir and Freundlich isotherm parameters for adsorption of Cr(VI) on WHB-GO.

Adsorbents	Langmuir model			Freundlich model		
	q_m (mg g ⁻¹)	K_L (L mg ⁻¹)	R^2	K_F (L mg ⁻¹)	n	R^2
30	124.17	0.045	0.95	32.38	4.52	0.98
40	131.49	0.070	0.94	40.67	5.05	0.98
50	150.51	0.060	0.90	52.89	5.75	0.98

Table 4 Thermodynamic parameters for Cr(VI) adsorption on WHB-GO.

Temperature (^o C)	$\ln K^0$	ΔG^0 (kJ mol ⁻¹)	ΔH^0 (kJ mol ⁻¹)	ΔS^0 (J K ⁻¹ mol ⁻¹)	R^2
30	-0.119	-2.239	31.265	102.009	0.988
40	0.226	-3.264			
50	0.650	-5.148			

Table 5 Adsorption capacities of different adsorbents for Cr(VI)

Adsorbents	q_{\max} (mg g ⁻¹)	Optimum pH	References
Saw dust activated carbon	65.8	2.0	1
Rice husk carbon	48.31	2.0	2
CCGO	67.66	2.0	3
PEI modified activated carbon	20.05	2.0	4
P4VP modified activated carbon	53.7	2.0	5
Zinc-biochar nanocomposites	102.66	2.0	6
WHB-GO	150.51	2.0	This study

1. T. Karthikeyan, S. Rajgopal and L. R. Miranda, *J Hazard Mater*, 2005, **124**, 192-199.
2. M. Bansal, D. Singh and V. K. Garg, *J Hazard Mater*, 2009, **171**, 83-92.
3. L. Li, L. Fan, M. Sun, H. Qiu, X. Li, H. Duan and C. Luo, *Colloids Surf B Biointerfaces*, 2013, **107**, 76-83.
4. M. Oowlad, M. K. Aroua and W. M. Wan Daud, *Bioresour Technol*, 2010, **101**, 5098-5103.
5. J. Fang, Z. Gu, D. Gang, C. Liu, E. S. Ilton and B. Deng, *Environmental science & technology*, 2007, **41**, 4748-4753.
6. C. Gan, Y. Liu, X. Tan, S. Wang, G. Zeng, B. Zheng, T. Li, Z. Jiang and W. Liu, *RSC Adv.*, 2015, **5**, 35107-35115.